Development of a High-resolution Fast Gamma-ray Imager for the New-generation PET III

Souichirou AOGAKI
Hideki KOTAKA
Ikuo MORITANI
Fujio TAKEUTCHI[1)]
Fumiharu Masafumi TOYAMA
[1)] Faculty of Science, Kyoto Sangyo University, Kyoto 603-8555 Japan
Faculty of Engineering, Kyoto Sangyo University, Kyoto 603-8555 Japan

Abstract

The disappearance of the air layer between scintillator crystals due to their sticking seems harmful. To avoid this phenomenon, an insertion of black flock paper is tried and the effect was studied. The result seems positive. But we need to look for a better material which is light tight, thin, solid yet not sticky.

I INTRODUCTION

We've pursued an experimental study on the development of the new PET (Positron-emission Tomography) device which is useful in medical treatment as well as for the brain research. However, the device is still expensive, and the main reason for that is the price for the Photomultiplier (PM) used for the read out of the small light signal. Our principal aim of the study is to develop a new device which is less expensive than the existing ones yet with a better spatial resolution. The main ingredient of the study is the use of Wave-length shifter (WLS) as light guides connecting optically the scintillator crystals and the PM[1]. The number of PM's in currently existing PET is proportional to the number of crystals, and this fact makes the device expensive, and limits the spatial resolution low, which is essentially dependent on the total num-

ber of crystals used. By using WLS as light guides, the number of PM's is proportional to the square root of the number of crystals, and this fact allows the use of much finer crystals than the ones used in the current PET.

Until now, we made pad out of crystals with polished surfaces without any material between them. According to the simulation which assumes totally flat parallel surfaces of crystals, the light emitted by the absorption of a gamma-ray in the middle of a crystal is transported by total reflection to the end of it, where the photons exit from the crystal to enter the light guide. This is the case for photons emitted with a sharp angle with respect to the side wall of the crystal, whereas, those emitted with nearly normal angle to the wall escape from the crystal, and enters the adjacent one through the air layer in-between, but they never fulfill the total-reflection condition so as to be transported to the end of the newly entered crystal, thus are considered to be lost. It was found, however, in the experimental study that this is not always the case. The discrepancy from the simulation might occur due to the disappearance of the air layer between crystals, which is caused by the application of pressure sideways when the crystal pad is built. That effect causes the optical contact of adjacent crystals, and the subdivision of the scintillator becomes meaningless.

Thus this time, we inserted a sheet of black paper between crystals and tried to find the effect of it. The paper used is a flock paper with a rough surface and cannot stick to the surface of the crystal. This paper used is relatively thick (0.25 mm) and the insertion of it increases the dead space of the gamma-ray detection. We plan to find a more appropriate material instead of this paper in the future if the result of the current test is promising.

In this report, we discuss the difference between crystal pad with and without black paper between the this crystals.

II SETUP

We used ^{22}Na beta+ source to obtain the gamma rays with an energy of 511 keV. The components of the experiment used in the study are described hereafter.

2.1 Scintillator crystal

We used this time LYSO (Ce) crystals as scintillator. The physical property as well as the dimensions of the crystals is shown in Table 1. As shown in Fig. 2.1, the crystals are bundled in a pad, and connected at each end, to an array of WLS, which transports the light to the PM.

Light Output [Photons/MeV]	32000
Wave length (Peak emission) [nm]	420
Decay time [ns]	41
Index of Refraction	1.81
Density [g/cm^3]	7.1
Effective Z	66.4
Dimensions [mm^3]	$1 \times 1 \times 20$

Table 1 The physical property and the dimensions of the LYSO(Ce) scintillator crystal used for this experiment

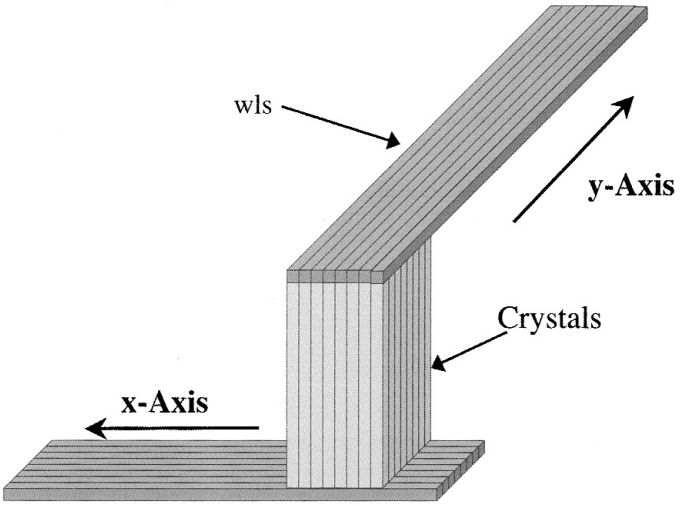

Fig. 2.1 Setup of a detector

2.2 Wave-length shifter (WLS)

The role of the WLS is to deflect 90 degrees the light exited from the end of a crystal in the direction of PM. It absorbs the light emitted by the LYSO crystal with a wave length of 440 nm and reemits light of about 500 nm. We used Y-11 multi-clad WLS with 1 mm diameter made by Kuraray[2] which showed a best performance in the past study [1]. Fig. 2.2 shows the absorption and emission spectra of this WLS.

2.3 Photomultiplier

We use HAMAMATSU H6568MOD position-sensitive photomultipliers which is a metal tube with 16 independent channels. The PM is modified so that one can obtain the last dynode signal, which is the sum of all the output signals from the 16 channels. The signal is positive, but we invert its polarity and read the pulse-height with CAMAC ADC.

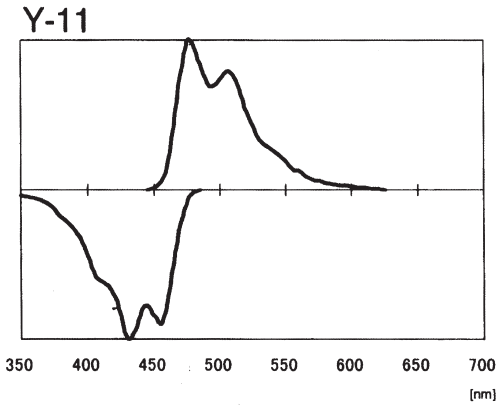

Fig. 2.2 Absorption and emission spectra of Y-11 WLS (from Kuraray catalog)

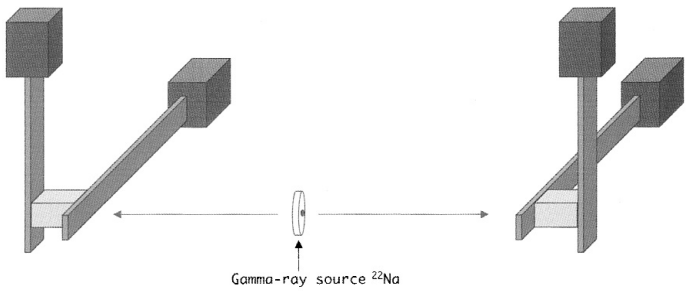

Fig. 2.3 Set up with two detectors in coincidence, and the gamma-ray source

2.4 Experimental setup

The experiment has been performed with two detectors placed on the opposite side of the gamma-ray source, as shown in Fig. 2.3. One detector pad consists of 13 by 13 crystal pieces in case the black paper was inserted, and 16 by 16 without paper. The pads were put in a frame made from an aluminum block. The cross section of the WLS is round, and to guarantee a better light transmission from the crystal to WLS, we used transparent adhesive tape [3]. The distance between the surface of the detector and the source was 12 cm on both sides.

The study of the light collection was made by irradiating the whole surface of the two detectors. As a Lu isotope contained in the scintillator has natural radioactivity, and thus to avoid the effect of it, the data have been obtained always with the two detectors in coincidence. The trigger signal was thus made from the coincidence of left and right signals, which are made as a coincidence between x and y last-dynode signals. The details are described in the reference [1]. The hit crystal is determined by the position of the WLS fired on x and y side. When more than one

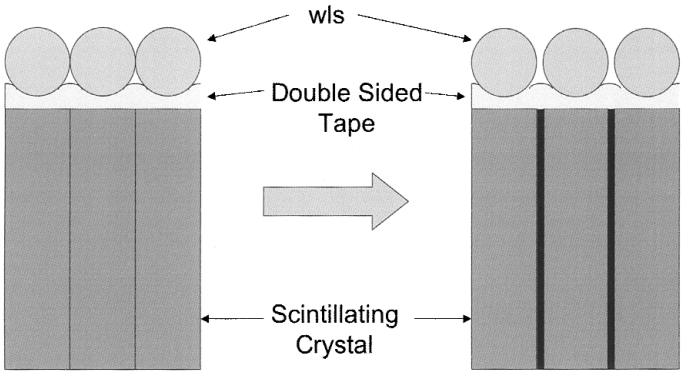

Fig. 2.4 Contact between the crystals and the WLS with 3M adhesive tape in-between

WLS fire in one event, we determine the hit position either with the WLS with a largest signal (simple maximum algorithm), or taking the weighted sum of the WLS signal (center of gravity algorithm). Fig. 2.4 shows the contact between the crystals and the WLS with 3M adhesive tape in-between.

III EXPERIMENTAL RESULTS

3.1 Measurement of the light amount in the total irradiation

3.1.1 Setup

As already described in the previous section, the measurement has been performed in the coincidence mode with the two detectors.

3.1.2 Results

Figs 3.1 and 3.2 shows the pulse-height distribution of the last dynode signal (x and y) from the pad with black paper. The same measurement was performed without black paper, and the results are shown in Figs. 3.3 and 3.4 for x and y, respectively. Here, the side y means the WLS array on the “front” side of the pad, which is the entrance of the gamma ray to the pad (closer to the radioactive source), and x, the opposite (back) side.

The average number of photoelectrons in each case was obtained using the method described in [1], and the results are summarize in Table 2. The table shows the ADC channel corresponding to the single photoelectron peak, the average of the light output, and the deduced number of photoelectrons. As already mentioned, the last-dynode signal is the sum of the signals

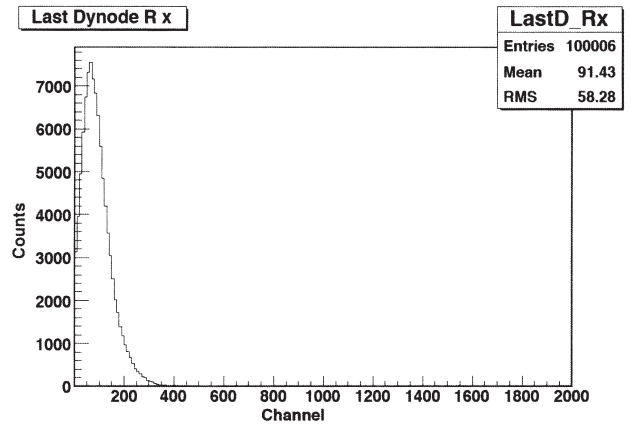

Fig. 3.1 Pulse-height distribution of the last dynode signal x from the pad with black paper

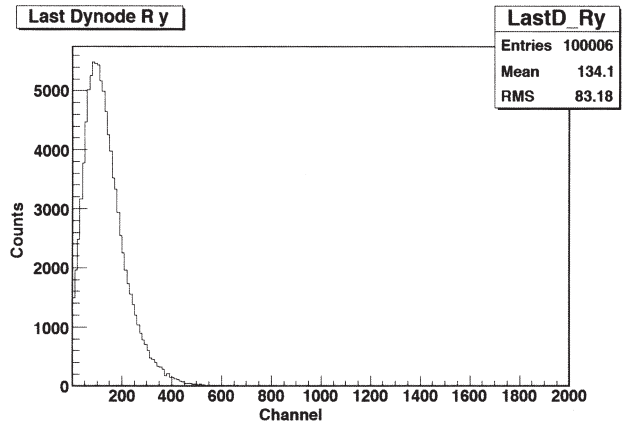

Fig. 3.2 Pulse-height distribution of the last dynode signal y from the pad with black paper

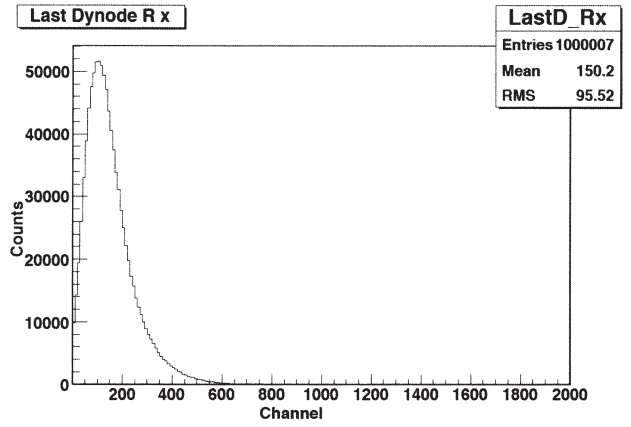

Fig. 3.3 Pulse-height distribution of the last dynode signal x from the pad without black paper

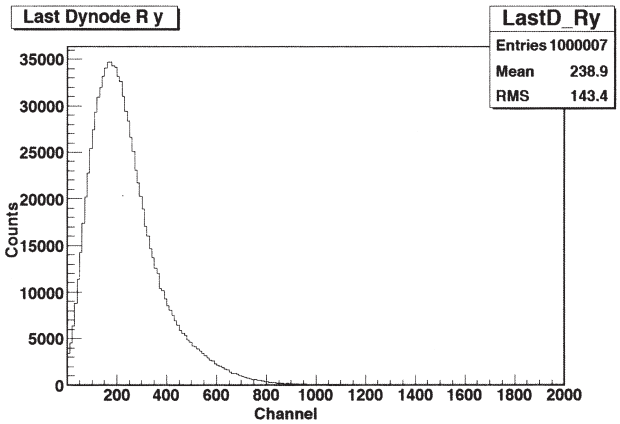

Fig. 3.4 Pulse-height distribution of the last dynode signal y from the pad without black paper

	Average of the histogram (chan)	Single photoelectron peak (chan)	Average number of photoelectrons
With black paper (x)	91.4	22.3	4.09
With black paper (y)	134.1	21.3	6.30
Without black paper (x)	150.2	22.3	6.72
Without black paper (y)	238.9	21.3	11.22

Table 2 The average number of photoelectrons in the Last Dynode signals are calculated using the average channels in the histograms and the spectra with single photoelectron peaks

from the crystals, if the photons are spread in many crystals, the total number of photons are recorded. In the case with black paper, the photons escaping from the side wall of the crystals are absorbed by the paper. Thus it seems reasonable that the average number of photoelectrons is smaller in this case. It is observed that the light coming out from the front side of the pad is always larger than the signal from the back side. According to the simulation result [1] using EGS [4] program, the absorption rate of the 511 keV gamma rays noticeably decreases with the depth of the scintillator, and almost 80% of the rays are absorbed with a scintillator of a depth (length) of 20 mm. Thus in a crystal, the light-emission points are distributed more intensely near the entrance (near WLS y) and this explains the difference of the light output between x and y layers.

Fig. 3.5 shows a typical light output from one crystal (anode signal) in the case with black paper. The same result without black paper is shown in Fig. 3.6. By using the method as above, the average number of photoelectrons are obtained and are shown in Table 3 for both with and without black paper. The average between all the crystals in the pads are:

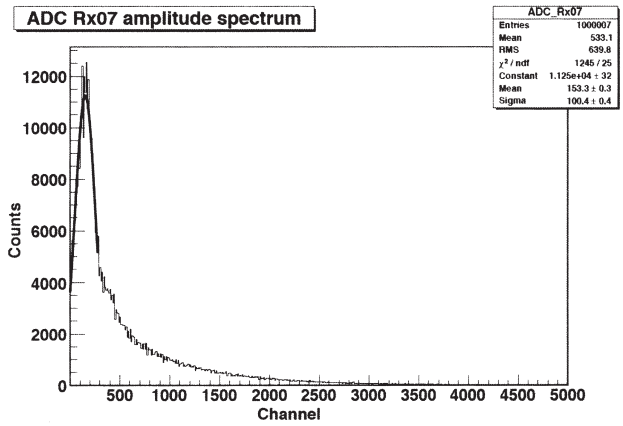

Fig. 3.5 Typical light output spectrum from one crystal (anode signal) in the case with black paper

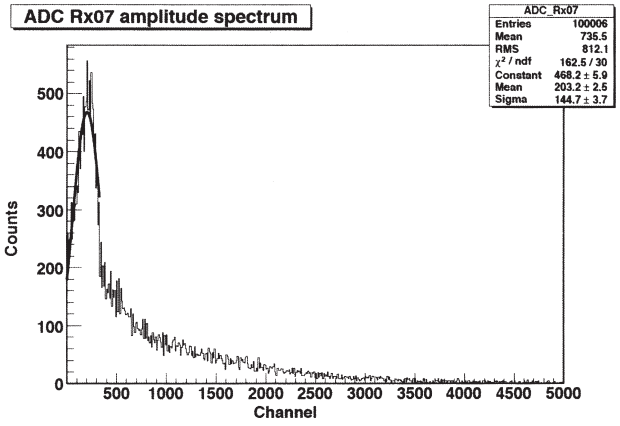

Fig. 3.6 Typical light output spectrum from one crystal (anode signal) in the case without black paper

with paper	3.55 ± 0.53 (front side y)	3.63 ± 0.57 (back side x)
without paper	2.76 ± 0.28 (front side y)	3.03 ± 0.35 (back side x)

As imagined from the fact that the last-dynode signal is larger with the pad without paper, whereas the anode signal is similar in the cases with and without paper, the average number of firing fibers is much larger in the case without paper. Without paper, 6.2 columns fire in average in one event, whereas 2.9 column fire in the case with black paper. The results are summarized in Table 4. Why is the average multiplicity more than one with black paper, which in principle should absorb all the photons escaping from the fired crystal? Compton scattering should be one of the reasons. But we cannot neglect the cross talk of the light at the level of the connection between the crystal and the WLS. The latter must be reduced in the future study. There can be also some cross talk at the level of the photocathode.

Without black paper (x)			
Column number	Average of the histogram (chan)	Single photoelectron peak (chan)	Average number of photoelectrons
1	442.5	152.8	2.90
2	422.6	152.7	2.77
3	425.9	145.5	2.93
4	315.3	151.7	2.08
5	311.8	107.7	2.89
6	559.0	167.5	3.34
7	623.0	181.2	3.44
8	533.1	158.2	3.37
9	435.3	117.8	3.69
10	555.6	182.8	3.04
11	597.0	197.2	3.03
12	430.7	146.1	2.95
13	476.7	173.9	2.74
14	472.7	153.9	3.07
15	509.9	165.3	3.08
16	543.9	168.0	3.24
Average			3.03 ± 0.35

Table 3-1 The average number of photoelectrons in the Anode signals are calculated using the average channels in the histograms and the spectra with single photoelectron peaks (x, without black paper)

Without black paper (y)			
Column number	Average of the histogram (chan)	Single photoelectron peak (chan)	Average number of photoelectrons
1	552.4	226.6	2.44
2	501.1	196.6	2.55
3	523.2	203.7	2.57
4	498.4	186.8	2.67
5	615.3	237.7	2.59
6	615.9	242.9	2.54
7	517.1	197.7	2.62
8	583.7	217.5	2.68
9	644.1	248.1	2.60
10	598.4	219.9	2.72
11	664.5	251.7	2.64
12	507.5	185.3	2.74
13	517.4	176.3	2.93
14	544.2	164.8	3.30
15	610.2	180.1	3.39
16	645.7	202.2	3.19
Average			2.76 ± 0.28

Table 3-2 The average number of photoelectrons in the Anode signals are calculated using the average channels in the histograms and the spectra with single photoelectron peaks (y, without black paper)

With black paper (x)			
Column number	Average of the histogram (chan)	Single photoelectron peak (chan)	Average number of photoelectrons
1	440.7	159.1	2.77
2	423.7	132.0	3.21
3	791.0	176.8	4.47
4	775.4	211.4	3.67
5	631.1	171.1	3.69
6	465.2	136.5	3.41
7	645.5	219.7	2.94
8	735.5	238.0	3.09
9	542.5	159.9	3.39
10	678.8	192.1	3.53
11	716.8	174.8	4.10
12	813.8	192.9	4.22
13	883.3	187.1	4.72
Average			3.63 ± 0.57

Table 3-3 The average number of photoelectrons in the Anode signals are calculated using the average channels in the histograms and the spectra with single photoelectron peaks (x, with black paper)

With black paper (y)			
Column number	Average of the histogram (chan)	Single photoelectron peak (chan)	Average number of photoelectrons
1	958.9	182.9	5.24
2	900.3	249.8	3.60
3	843.4	245.1	3.44
4	710.3	208.4	3.41
5	789.3	231.8	3.40
6	851.4	258.9	3.29
7	744.3	231.6	3.21
8	808.1	264.9	3.05
9	603.2	180.2	3.35
10	677.9	197.6	3.43
11	638.9	170.4	3.75
12	635.7	196.6	3.23
13	784.2	207.3	3.78
Average			3.55 ± 0.53

Table 3-4 The average number of photoelectrons in the Anode signals are calculated using the average channels in the histograms and the spectra with single photoelectron peaks (y, with black paper)

	With black paper x	With black paper y	Without black paper x	Without black paper y
Average number of photoelectrons (Anodes)	3.63	3.55	3.03	2.76
Average multiplicity	3.00	2.74	6.29	6.17
Average number of photoelctrons (Last Dynodes)	4.09	6.30	6.72	11.22

Table 4 Comparison of the results with and without black paper with respect to the average amount of light from the anodes, average multiplicity and the amount of light from the Last Dynodes

3.2 Measurement of the spatial resolution using a collimator

3.2.1 Setup

As shown in Fig. 3.7, a collimator with a slit of 0.5 mm width was placed in front of one of the detectors. The collimator limits the irradiation by the gamma rays to one array of the pad on the detector on which the collimator is placed. Fig. 3.8 shows the TDC spectrum of the time difference between the two last dynodes x and y of one detector (without paper). For the further analysis, only events within the window (width: 160 ns considering the decay time) have been used. The time difference between two counters shown in Fig. 3.9 shows a width of 7.05 ns RMS. Events within the coincidence time window of 500 - 2500 channels have been used for the analysis.

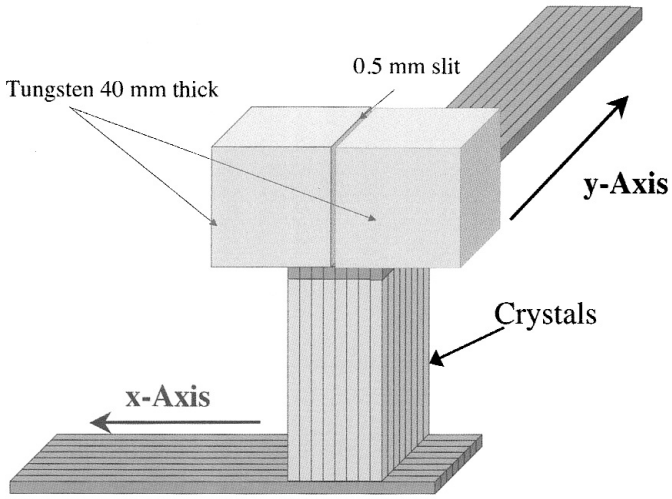

Fig. 3.7 Setup of a measurement with a collimator in front of one of the detectors

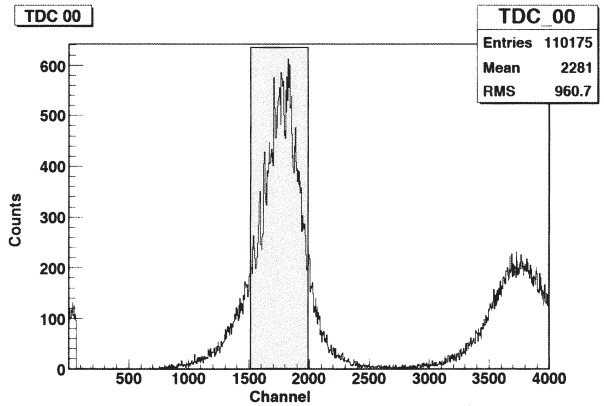

Fig. 3.8 TDC spectrum of the time difference between the two last dynodes x and y of a detector (without paper) (48.8 ps/chan)

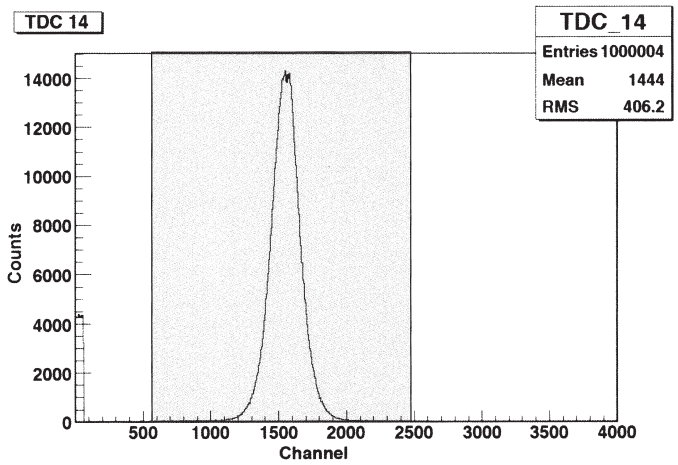

Fig. 3.9 TDC spectrum of the time difference between the two detectors (48.8 ps/chan)

3.2.2 Spatial resolution

Fig. 3.10 shows the 2-dimensional histogram of the events recorded by the detector with the collimator in front. This is for the case of no black paper. For the events with multiple WLS firing, the simple maximum algorithm has been used for the reconstruction. One can clearly see the image of the slit in the histogram. Fig. 3.11 shows the same histogram but taken with the pad with black paper. The image of the slit looks narrower. The projection of these 2-dimensional histograms (Figs. 3.10 and 3.11) to the vertical axis are shown in Figs. 3.12 and 3.13, respectively. The obtained histograms are fitted with a Gaussian plus a constant (with 4 parameters) such as

$$p_0 e^{-(x-p_1)^2/2p_2^2}.$$

Here the unit of x is the interval between crystals, namely, in the case without paper is 1 mm, whereas in the case with paper, it is 1.23 mm. Thus the width of the peak (FWHM) is 1.63 mm in the case without paper, and 1.68 mm with paper. The difference is small. The light spread due to the optical contact of adjacent crystals does not affect the spatial resolution as far as we use the simple maximum algorithm. It should, however, be noted that the background constant (p_3) in the fits in Figs. 3.12 and 3.13, is noticeably smaller in the case with paper.

Also the average number of fired columns as shown in Fig. 3.14 (without paper) and in Fig. 3.15 (with paper) shows a clear difference between these two cases. We see in fact that most of the time, only 2 to 3 columns fire simultaneously with the paper.

In Fig. 3.16, which shows the spread of the fired columns (distance between the most distant fired columns) as a function of the multiplicity in the case with paper, we see that in the case of multiplicity 2 or 3, the fired columns are adjacent, whereas in the higher multiplicity case, there

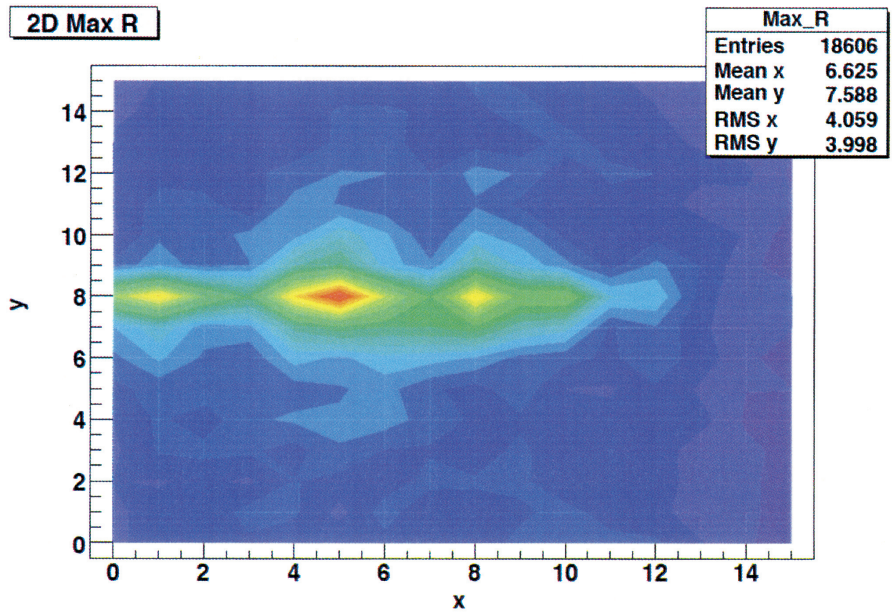

Fig. 3.10 Two-dimensional histogram of the events recorded by the detector with the collimator in front (without black paper)

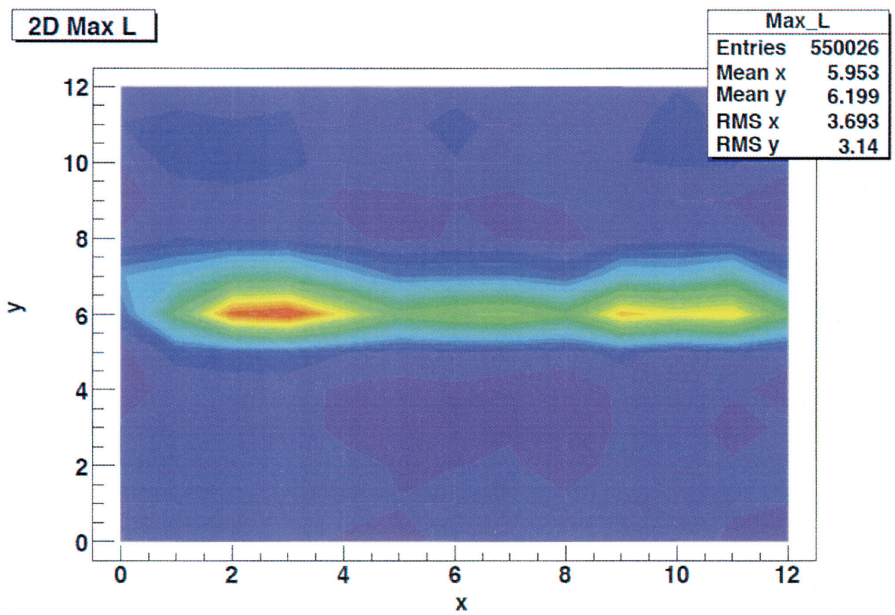

Fig. 3.11 Two-dimensional histogram of the events recorded by the detector with the collimator in front (with black paper)

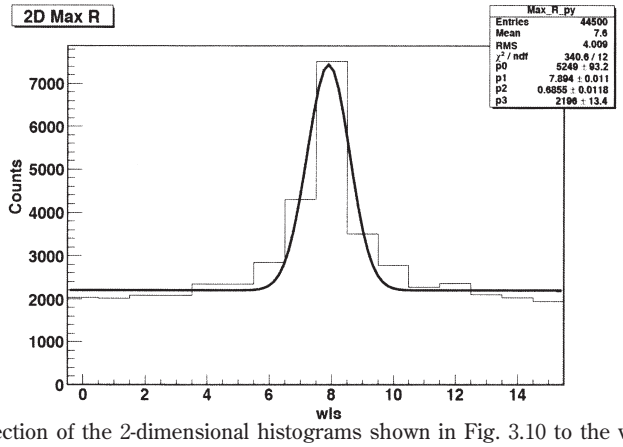

Fig. 3.12 The projection of the 2-dimensional histograms shown in Fig. 3.10 to the vertical axis (without black paper)

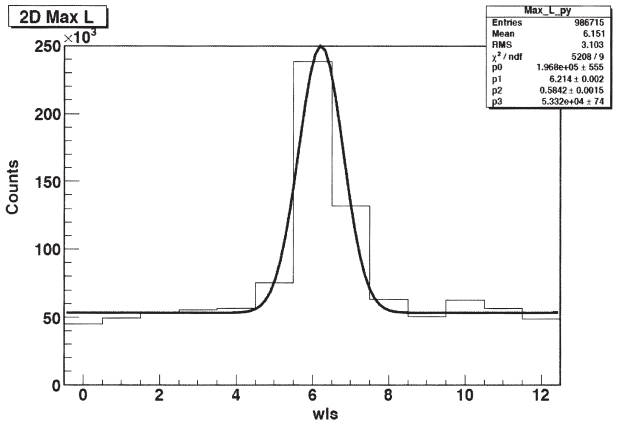

Fig. 3.13 The projection of the 2-dimensional histograms shown in Fig. 3.11 to the vertical axis (with black paper)

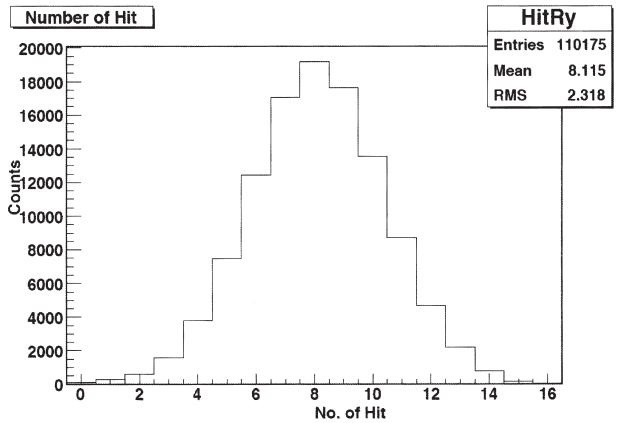

Fig. 3.14 Average number of fired columns (without black paper)

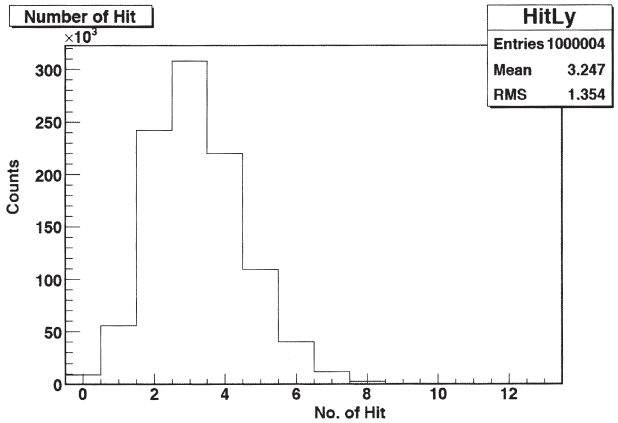

Fig. 3.15 Average number of fired columns (with black paper)

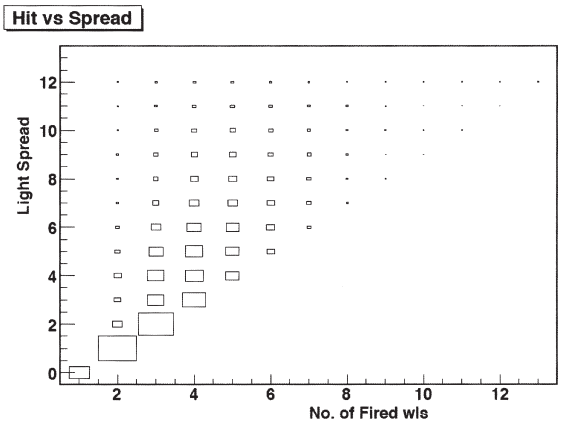

Fig. 3.16 Spread of the fired columns (distance between the most distant fired columns) as a function of the multiplicity (with black paper)

are unfired columns in-between. Assuming that in the case with paper, events which fire more than 3 columns are due to some kind of remote cross talk (including Compton scattering), we tried to see if one can obtain a better spatial resolution by excluding those events. In Fig. 3.17 the events are plotted as a function of the weighted average of those up to 4 columns fired (center of gravity algorithm). The binning chosen is 1/10 of the crystal spacing, thus 0.123 mm. The fitted curve shows a FWHM of 0.75 mm which is a very good a spatial resolution.

We try to make the same kind of exercise in the case without paper.

In Fig. 3.19, the events are plotted as a function of the center of gravity of the multiple hits in the cases of multiplicity 1, 2, 3, 4, 5, 6, 7 and 8. It is surprising that the image of the slit is hardly visible when the multiplicity is 1 or 2. Cleaner peak is visible in the case of multiplicity 7 or 8. But as shown in Fig. 3.18, when the spread becomes large, the cluster of fired columns contain non-

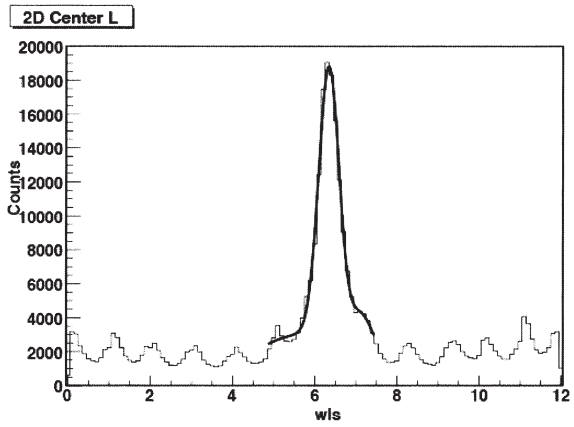

Fig. 3.17 Events up to 4 columns fired are plotted as a function of the weighted average of fired columns (center of gravity algorithm)

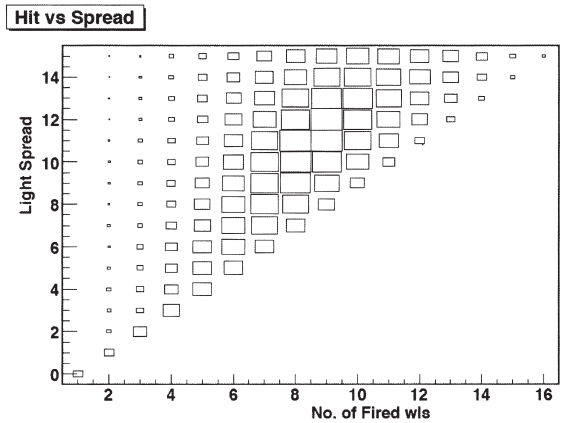

Fig. 3.18 Spread of the fired columns (distance between the most distant fired columns) as a function of the multiplicity (without black paper)

fired columns in between, and the final resolution can not be very good. It should be noted that when the multiplicity is high, the pulse height in each anode is small, and the hits are scattered randomly which results in a peak in the middle. That means the central peak does not necessarily mean the image of the slit. Also it should be noted that we observe 2 peaks near the end of the histograms in addition to the central peak, in the case of small multiplicity. These are the areas which are totally covered with the tungsten collimator, and thus must be due to some optical phenomenon. This effect is yet to be investigated.

IV DISCUSSION

It is clear that there is a discrepancy between the real observation and the result of a simula-

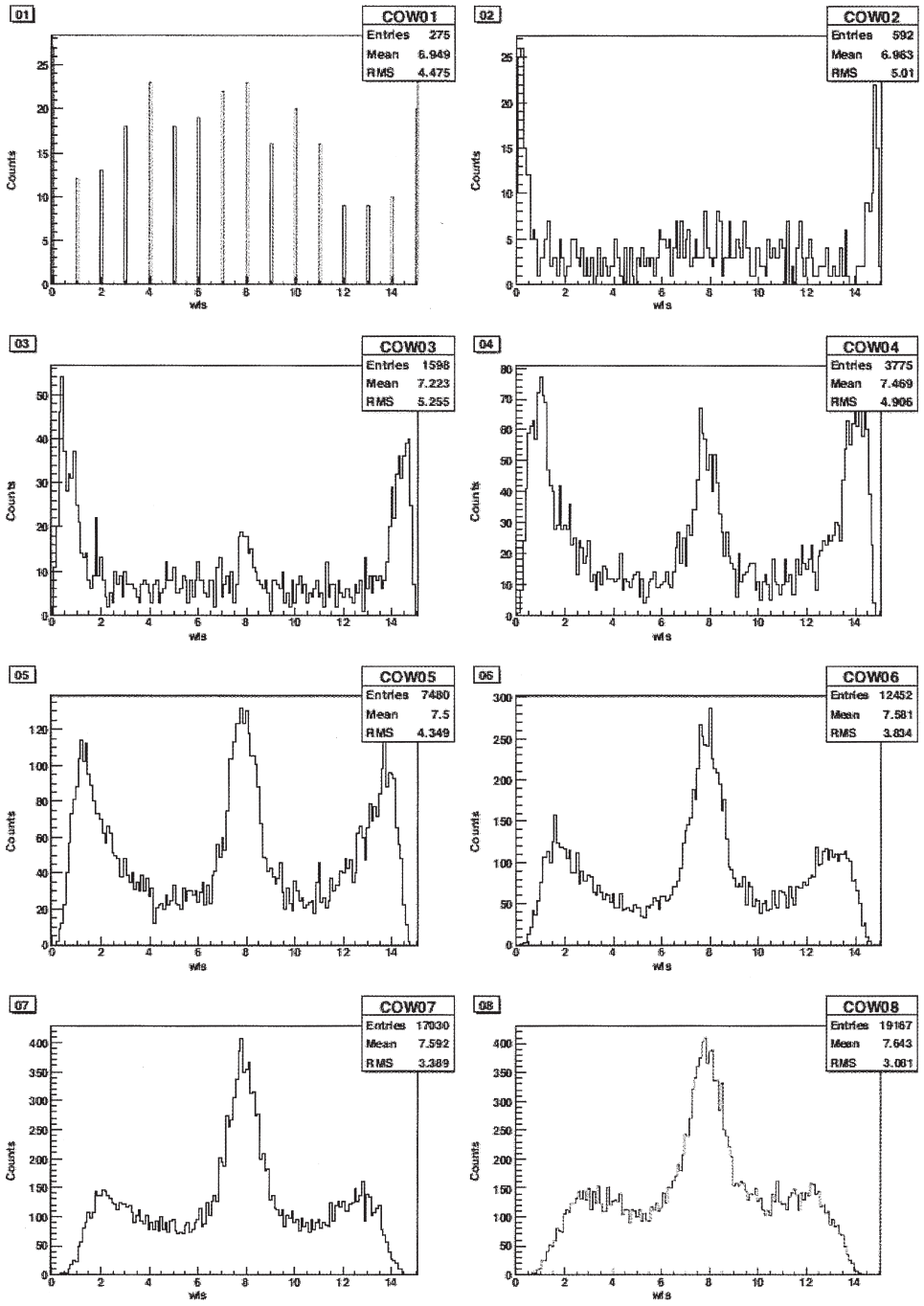

Fig. 3.19 Events are plotted as a function of the center of gravity of the multiple hits in the cases of multiplicity 1, 2, 3, 4, 5, 6, 7 and 8 (without black paper)

tion in which one assumes an existence of air layers between crystals. Furthermore, the disappearance of the air layer gives a bad effect. To avoid this effect, we used a black flock paper in this study. We could see that this can improve the situation in many respects, as discussed in the previous chapter. But as the paper is relatively thick, one cannot avoid an increase of the dead space. Furthermore this flock paper is rather soft. Therefore the definition of the position of each crystal unit becomes ambiguous. This can cause the geometrical matching of the crystal ends to the WLS more problematic. Thus we need to find a material which is thin and optically opaque and physically solid yet does not stick to the surface of the crystal.

References

[1] F. Takeutchi and S. Aogaki; Read-out of a YAP array detector using wave-length shifter, Proc. Intern. mini-Workshop for Scintillating Crystals and their Applications Nov. 2003, KEK Japan (2004) 213-218,
F. Takeutchi and S. Aogaki; Read-out of scintillator crystal matrix using wave-length shifter, Proceedings of the Eighth International Conference on Inorganic Scintillator and their Use in Scientific and Industrial Applications, SCINT2005 at Crimea, Sept. 2005. Proceedings pp 298-302,
F. Takeutchi and S. Aogaki; Development of a High-resolution Fast Gamma-ray Imager for the New-generation PET, Bull. Res. Inst. Advanced Tech., Kyoto Sangyo University Vol. **4** (2005) 45 - 68
K. Inoue et al.; Development of a High-resolution Fast Gamma-ray Imager for the New-generation PET II, Bull. Res. Inst. Advanced Tech., Kyoto Sangyo University Vol. **5** (2006) 97 - 124
F. Takeutchi and S. Aogaki; Read-out of YAP and LuYAP crystal matrix using wave-length shifter, Bull. Res. Inst. Advanced Tech., Kyoto Sangyo University Vol. **5** (2006) 85 - 96
[2] Catalog Kuraray Japan
[3] 3M, http://www.mmm.co.jp/tape-adh/
[4] EGS, http://www.slac.stanford.edu/egs/